JGR Earth Surface

RESEARCH ARTICLE

Key Points:

- Ice-marginal moraines in the upper Khumbu Valley represent a complete record of regional glacier change between 7.4 ka and the present day
- Moraine building modified the response of Khumbu Glacier to climate change after 8 ka
- Holocene moraine volume indicates a catchment-wide denudation rate of 0.8–1.4 mm per year

Be-10 Dating of Ice-Marginal Moraines in the Khumbu Valley, Nepal, Central Himalaya, Reveals the Response of Monsoon-Influenced Glaciers to Holocene Climate Change

Josephine Hornsey[1], Ann V. Rowan[1,2], Martin P. Kirkbride[3], Stephen J. Livingstone[1], Derek Fabel[4], Angel Rodes[4], Duncan J. Quincey[5], Bryn Hubbard[6], and Vincent Jomelli[7]

[1]Department of Geography, University of Sheffield, Sheffield, UK, [2]Department of Earth Science, University of Bergen and Bjerknes Centre for Climate Research, Bergen, Norway, [3]Geography and Environmental Science, University of Dundee, Scotland, UK, [4]Scottish Universities Environmental Research Centre, East Kilbride, UK, [5]School of Geography, University of Leeds, Leeds, UK, [6]Centre for Glaciology, Department of Geography and Earth Sciences, Aberystwyth University, Aberystwyth, UK, [7]Aix-Marseille University, CNRS, IRD, INRA, Coll France, UM 34 CEREGE, Technopôle de l'Environnement Arbois-Méditerranée, Aix-en-Provence, France

Abstract The dynamic response of large mountain glaciers to climatic forcing operates over timescales of several centuries and therefore understanding how these glaciers change requires observations of their behavior through the Holocene. We used Be-10 exposure-age dating and geomorphological mapping to constrain the evolution of glaciers in the Khumbu Valley in the Everest region of Nepal. Khumbu and Lobuche Glaciers are surrounded by high-relief lateral and terminal moraines from which seven glacial stages were identified and dated to 7.4 ± 0.2, 5.0 ± 0.3, 3.9 ± 0.1, 2.8 ± 0.2, 1.3 ± 0.1, 0.9 ± 0.02, and 0.6 ± 0.16 ka. These stages correlate to each of the seven latest Holocene regional glacial stages identified across the monsoon-influenced Himalaya, demonstrating that a coherent record of high elevation terrestrial palaeoclimate change can be extracted from dynamic mountain landscapes. The time-constrained moraine complex represents a catchment-wide denudation rate of 0.8–1.4 mm a^{-1} over the last 8 kyr. The geometry of the ablation area of Khumbu Glacier changed around 4 ka from a broad, shallow ice tongue to become narrower and thicker as restricted by the topographic barrier of the terminal moraine complex.

Plain Language Summary Satellite observations indicate that glaciers in the monsoon-influenced Himalaya are changing rapidly in response to climate change. However, understanding why glaciers are changing requires observing glacier behavior over longer timescales using the glacial geological record. We mapped the geometry and measured the ages of ice-marginal moraines built by two adjacent glaciers in the Everest region of Nepal. The moraines represent a complete record of glacier expansion during cold periods in the monsoon-influenced Himalayan region over the last 8,000 years. Moraines formed by the large Khumbu Glacier and the smaller, steeper Lobuche Glacier also reveal differences in how these glaciers have changed since the last Ice Age. The results are useful to understand how monsoon-influenced Himalayan glaciers respond to climate change, and to improve projections of their future behavior.

1. Introduction

Glaciers in the monsoon-influenced Himalaya have undergone rapid changes in their mass and dynamic behavior during the Holocene (Murari et al., 2014; Saha et al., 2019; Solomina et al., 2015, 2016). Recent satellite observations suggest rapid glacier mass loss, and that debris-covered and clean-ice glaciers lose mass at similar rates (Hugonnet et al., 2021). However, a limitation of such remote-sensing observations is that they represent a relatively short timescale (decades) compared to the response times of mountain glaciers to climatic forcing (centuries) (Hambrey et al., 2008). Understanding the processes that affect how glaciers have responded to climate change through the Holocene (~11 ka to present) is required to identify the drivers of longer-term change and constrain projections of future glacier evolution (Nicholson et al., 2021; Owen et al., 2009; Rowan et al., 2015).

More than a thousand moraine ages produced using terrestrial cosmogenic nuclide exposure-age dating constrain multiple regional stages of Quaternary glaciation in the monsoon-influenced Central Himalaya, termed monsoonal Himalayan–Tibetan stages (Murari et al., 2014). The moraine ages indicate 13 regional glacial stages during the Last Glacial from 91 ± 15 to 12.9 ± 0.9 ka, and 11 regional stages during the Holocene from 11.4 ± 0.7 to

Methodology: Josephine Hornsey, Derek Fabel, Angel Rodes, Vincent Jomelli
Project Administration: Vincent Jomelli
Software: Angel Rodes
Supervision: Ann V. Rowan, Martin P. Kirkbride, Stephen J. Livingstone, Derek Fabel, Angel Rodes, Duncan J. Quincey
Validation: Josephine Hornsey, Derek Fabel, Angel Rodes, Vincent Jomelli
Visualization: Josephine Hornsey
Writing – original draft: Josephine Hornsey, Ann V. Rowan
Writing – review & editing: Ann V. Rowan, Martin P. Kirkbride, Stephen J. Livingstone, Derek Fabel, Angel Rodes, Duncan J. Quincey, Bryn Hubbard, Vincent Jomelli

0.4 ± 0.1 ka (Murari et al., 2014; Saha et al., 2018). Identification of the timing of moraine building by individual glaciers within the same valley can be informative in determining the timing of local stages of glacier expansion, both for comparison with regional glacial stages and to identify the processes that result in differing responses of adjacent glaciers to the same change in palaeoclimate. Past glacier volume can be inferred from the position of terminal and lateral moraine crests (e.g., Braumann et al., 2021; Solomina et al., 2015). The timing of moraine formation and the rate of glacier change can be determined by dating boulders exposed on the crests of ice-marginal moraines (Balco, 2020). Be-10 in quartz is particularly useful in young glacial environments as the well-defined production rate and can give precise results when dating surfaces with an exposure history of several hundreds of years (e.g., Saha et al., 2016, 2018).

Glaciers in the Khumbu Valley, Nepal, in common with those elsewhere in the Central Himalaya, fluctuated during the Late Quaternary and Holocene and formed substantial ice-marginal moraines (Finkel et al., 2003; Owen et al., 2009). Previous studies have investigated the timing of moraine building in the Khumbu Valley to constrain the timing of the local Last Glacial Maximum (LGM) to two stages: 24.4 ± 1.2 and 17.1 ± 0.3 ka, with three subsequent periods of moraine building identified at 11.5 ± 0.2, 4.5 ± 0.1, and 1.3 ± 0.3 ka (Figure 1; Finkel et al., 2003). The periods of Holocene glacier expansion are synchronous with three of the regional glacial stages but the remaining stages have not been identified in the Khumbu Valley.

In tectonically active glacierised settings such as the Himalaya, glaciers can build high-relief moraines due to the substantial volume of sediment produced by glacial and periglacial erosion (Heimsath & McGlynn, 2008; Scherler, 2014). When sediment supply to a glacier exceeds the rate of sediment evacuation to moraines, a supraglacial debris layer may develop from the glacier terminus and extend across the ablation area (Anderson & Anderson, 2018; Benn et al., 2012; Kirkbride, 2000). Supraglacial debris thicker than a few centimeters reduces ablation, allowing the glacier tongue to persist at a lower elevation than a climatically equivalent clean-ice surface (Anderson et al., 2021; Nicholson & Benn, 2013; Rounce et al., 2018). Glaciers in the Khumbu Valley are currently mantled by extensive debris layers that formed in response to recent mass loss (Herreid & Pellicciotti, 2020; Rowan et al., 2015). During periods of glacier expansion, the majority of supraglacial debris forms ice-marginal moraines that indicate periods of ice-margin stability exceeding the transient response of the glacier to a change in mass balance (Rowan et al., 2022).

We quantified the timing of Holocene moraine building by two adjacent glaciers in the upper Khumbu Valley to identify if their response to regional palaeoclimate change differed due to glaciological controls. Khumbu Glacier and Lobuche Glacier occupy the same valley and have therefore undergone similar climatic forcing, but differ from each other in their geometry and dynamic behavior. The moraine geochronology is used to constrain the inception of the Holocene moraine complex and the sediment volume is then used to estimate of the long-term catchment-wide denudation rate.

2. Field Site

The upper Khumbu Valley forms part of the headwaters of the Dudh Koshi that is a major tributary of the Ganges (Figure 1; Hambrey et al., 2008; Owen et al., 2009). Khumbu Glacier is 16 km long and 19 km^2 in area with a low-angle tongue and a median elevation of 5,570 m above sea level (a.s.l.) (RGI Consortium, 2017). Extensive lateral and terminal moraines surround the glacier and merge with the debris-covered terminus. The present-day glacier is mantled with rock debris up to several meters thick near the terminus that generally thins up-glacier (Rowan et al., 2021). Changri Nup Glacier and Changri Shar Glacier are former tributaries; satellite imagery indicates that they were confluent with Khumbu Glacier until at least 1984 CE. Lobuche Glacier is 2 km long and 0.9 km^2 in area with a relatively steep surface. The active glacier ranges in elevation from 5,060 to 5,850 m a.s.l. (RGI Consortium, 2017) and is detached from the former debris-covered tongue, which is surrounded by closely spaced lateral and terminal moraines. Geodetic mass balance for glaciers in this region was estimated as -0.38 ± 0.11 m water equivalent a^{-1} from 2009 to 2018 (King et al., 2020). The equilibrium line altitude of debris-covered glaciers is difficult to infer from their geometry, as heavily debris mantled termini persist at lower elevations than would be possible for climatically equivalent clean-ice glaciers, but is estimated from numerical modeling as being above 6,000 m a.s.l. (Rowan et al., 2021).
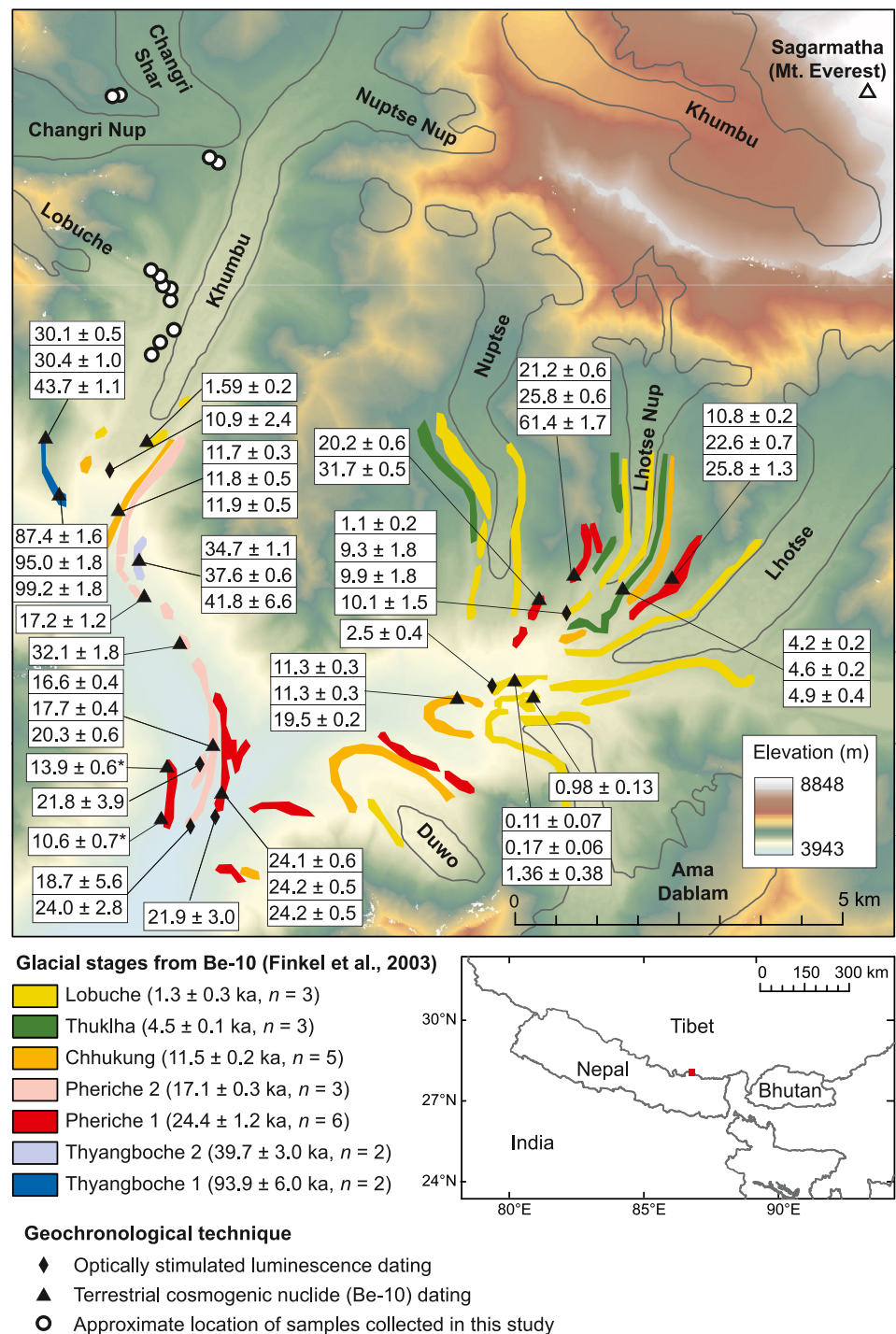
Figure 1. Map of moraine crests and the previous geochronology for the upper Khumbu Valley (Finkel et al., 2003; Richards, 2000; Richards et al., 2000; Rowan, 2017). Ages (in ka) were measured using Be-10 exposure-age dating of moraine crests (Finkel et al., 2003; Owen et al., 2009) and OSL dating of glacial sediments (Richards, 2000; Richards et al., 2000). The ages for each glacial stage are the error-weighted mean of sample ages with the standard deviation of the internal uncertainties from Finkel et al. (2003) after recalibration and a chi-squared test to identify outliers. The two Be-10 ages identified with an asterisk are presented in Finkel et al. (2003) but produced by Aoki and Imamura (1999). The underlying image is the 8-m High Mountain Asia Digital Elevation Model (Shean, 2017) and glacier outlines from the Randolph Glacier Inventory (RGI Consortium, 2017).

3. Methods

3.1. Geomorphological Mapping

Geomorphological mapping was undertaken using the 8-m High Mountain Asia Digital Elevation Model (DEM; Shean, 2017) and satellite imagery from ALOS PRISM (2.5-m resolution; panchromatic) and Google Earth. Shaded relief maps and slope maps were produced from the DEM to minimize directional bias when identifying and mapping landforms (Smith & Clark, 2005). These images were interpreted qualitatively alongside photographs from previous field expeditions (Figure 2) to identify moraine crests (Figure 3). Some moraine surfaces host low-lying vegetation that was used to distinguish between moraines of different ages. Unvegetated moraine surfaces composed of loose sediment are generally younger than surfaces where fine-grained sediment supports a sparse covering of grasses, mosses and occasional small shrubs. The moraines are composed of a mixture of clasts of leucogranite and sillimanite gneiss (Searle et al., 2003), which are visually similar at this scale and cannot be used to define individual landforms. Moraine crests were identified and mapped as polylines in ESRI ArcMap (v.10.7) according to their morphology, proximity to glaciers, areas prone to slope collapse, and areas modified by fluvial activity. The mapping was evaluated and refined using field observations in April–May 2018.

3.2. Be-10 Exposure-Age Dating

Moraine crests were examined in the field to ensure they were undisturbed since deposition (Kirkbride & Winkler, 2012). We collected 3–5 boulders per moraine to increase the likelihood of age clustering and hence the precision of the resulting landform ages (Balco, 2011; Owen & Dortch, 2014). Boulders on the moraine crests were chosen to ensure that they represented the last phase of moraine building (Kirkbride & Winkler, 2012). Large, flat-topped boulders were selected to ensure limited topographic shielding and minimal post-depositional movement (Heyman et al., 2016). Vegetation cover was insufficient to cause any shielding of the boulders sampled. Samples were collected from boulders composed of either leucogranite or sillimanite gneiss, which are compositionally similar but differ texturally.

Thirty-three samples were collected from boulders embedded in the crests of four moraines formed by Khumbu and Changri Nup Glaciers and three formed by Lobuche Glacier (Table 1). About 1 kg of rock was collected from the uppermost 0.04 m of each boulder by hand using a hammer and chisel to minimize self-shielding of the sample and environmental damage. The samples were crushed and sieved to separate the grains. The 250–500 μm fraction was washed, dried, and separated magnetically to recover the non-magnetic component. The samples were placed in a 6:1:1 solution of water, 37% HCl and 68% HNO_3 (aqua regia) on a hot plate (50°C) to remove organic matter, carbonates and soluble oxides. A mixture of 100:1 of water to concentrated (40%) HF was used to etch the feldspar and mica grains slightly, helped by placing on a shaker table for 1 hr. The sample was then mixed with eucalyptus oil and placed into a surfactant solution to remove feldspar and mica grains by froth flotation (Herber, 1969). The floating minerals were discarded, and the remaining quartz grains recovered and placed into a solution of water, HF (40%), and HNO_3 at a ratio of 150:2:1 in a high-power ultrasonic tank for 24 hr, repeated three times to remove meteoric ^{10}Be by isolating the quartz grain cores.

An aliquot of the quartz cores was sampled and tested for purity by dissolving and measuring the content of Al, Be, Fe, Ca, and Ti using ICP-OES. Samples that were not considered sufficiently pure were returned to the water, HF, and HNO_3 solution. Samples containing less than 175 ppm Al were dissolved in pure HF, and each sample spiked with 0.2 mg of ^9Be using an in-house carrier solution obtained from Phenakite. Once dissolved, the samples were dried to evaporate HF and converted to a chloride by the addition of HCl. The samples were then passed through an anion exchange chromatography column to remove Fe. The Fe-free samples were dried to evaporate all the HCl, and H_2SO_4 was added to convert the sample into a sulfate. The sample was then passed through a cation exchange chromatography column to remove the Ti and B, and to separate out the Al and Be fractions, eluted using HCl solutions. The remaining Be fractions were precipitated as hydroxides, and then oxidized at 900°C. The subsequent BeO was mixed with Nb at a ratio of 1:6 and pressed into copper cathodes for Accelerator Mass Spectrometer (AMS) analysis (Mendelová et al., 2020; Xu et al., 2010).

Twenty-five samples were measured at the Scottish Universities Environmental Research Center AMS facility. ^{10}Be concentrations ranged between 2.06×10^{-14} and 7.43×10^{-12} $^{10}Be/^9Be$ and were scaled to a nominal value of 2.79×10^{-11} $^{10}Be/^9Be$ or NIST SRM4325 standard (Nishiizumi et al., 2007). Procedural blank measurements

Figure 2.

ranged between 0.06% and 21% of the sample $^{10}Be/^9Be$ ratios. Eight samples (PYR1, PYR2, PYR3, PYR4, NEP10, NEP11, NEP12, and NEP14B) were analyzed using AMS at Center Européen de Recherche et D'enseignement des Géosciences De L'Environnement, Aix-en-Provence, France. Measurements were calibrated against the in-house standard STD-11 with an assigned $^{10}Be/^9Be$ ratio of $1.191 \pm 0.013 \times 10^{-11}$ (Braucher et al., 2015) using a ^{10}Be half-life of $1.387 \pm 0.0012 \times 10^6$ years (Chmeleff et al., 2010). The uncertainty of these corrections is included in the stated standard internal uncertainties. External uncertainties including the production rate and scaling uncertainties give a systematic uncertainty of $\pm4.8\%$ for the data set.

Exposure ages for each sample were calculated using the online cosmogenic nuclide exposure-age calculator v.3 (Balco et al., 2008) with a global production rate (Borchers et al., 2016) and the Lifton/Sato scaling method (Lifton et al., 2014). Topographic shielding calculated from the 8-m DEM compared favorably with skyline measurements made in the field. Field measurements were not used as low cloud frequently limited visibility of the skyline. For each sample, a rock density of 2.65 g cm^{-3} was used and the erosion rate was assumed to be zero due to the resistant nature of the boulder surfaces, in line with Finkel et al. (2003) who estimated that an erosion rate of 1–5 mm a^{-1} would result in underestimation of an age of 1%–4%. We did not apply a snow-cover correction because the moraine crests are often windswept and shed snow efficiently, while the present-day snowpack in this region is thin (Owen et al., 2009). A chi-squared test identified possible outliers from the sample ages for each moraine (Balco et al., 2008). The ages can be recalculated using different scaling protocols and production rate calibrations through the Informal Cosmogenic Nuclide Exposure-age Database (https://version2.ice-d.org/alpine/).

4. Results

Moraines were numbered sequentially from the most proximal to the most distal for each glacier. Moraine exposure ages are reported as the error-weighted mean of the samples from each moraine with the internal uncertainty given as one standard deviation of the mean to a 95% confidence interval, except for the Lobuche 2 moraine for which the confidence interval was lower and so the standard error is used (Table 1, Figure 4).

4.1. Khumbu Glacier Moraines and Geochronology

Khumbu Glacier is bounded by seven distinct lateral moraines, the Khumbu 1–7 moraines, with each crest separated by 50–100 m horizontally (Figures 3 and 4a). The terminal moraine is over 500 m wide with a frontal ramp 250 m in relief and two distinct crests identified as the Khumbu 2 and Khumbu 6 moraines (Figure 2b). Close to the present-day glacier, the terminal moraine contains multiple small ice-cored ridges, indicating that the formation of this moraine was accompanied by substantial glacier thickening resulting from strong compressive flow at the terminus (Hambrey et al., 2008). The debris-covered tongue has receded 1–2 km from the terminal moraine, with the area immediately inside the moraine occupied by ice-cored debris and stagnant ice with a similar surface elevation to the terminal moraine crest (Figure 2c).

The Khumbu 1 lateral moraine is fragmented and only identifiable from 1 to 2 km up-glacier from the terminus and south of Changri Nup Glacier (Figure 2f). The Khumbu 1 moraine has unvegetated surfaces and unstable proximal slopes with crest heights up to 40 m above the current glacier surface and much lower than the Khumbu 2 moraine. This moraine is undated but may be similar in age to the Changri Nup 1 moraine.

The Khumbu 2 lateral moraine is nearly continuous for 8–9 km between the terminal moraine and the upper ablation area (Figures 2c and 2g) with an asymmetrical cross-profile such that the distal surfaces are stable, vegetated and dissected by relict gullies, while the proximal slopes are steep and actively backwasting. The relief of the lateral moraine crest varies from 60 m above the valley floor at about 1 km from the terminal moraine up to 200 m further upglacier. The true-left lateral moraine has one distinct crest, indicating that the three cirque glaciers on this side of the valley disconnected prior to the formation of this moraine. Three samples (KH1, KH2, and KH3)

Figure 2. Photographs of moraines in the upper Khumbu Valley and boulders sampled for Be-10 exposure-age dating. (a) The Last Glacial Maximum Pheriche moraines formed by Khumbu Glacier looking downvalley, (b) the Last Glacial and Holocene terminal moraines of Khumbu Glacier looking upvalley, (c) the Holocene Khumbu and Lobuche Glacier moraines looking downvalley, (d) the Changi Shar Glacier moraines looking across the former glacier ablation area to the south, (e) the Changi Nup Glacier moraines looking across the former glacier ablation area to the north, (f) the Khumbu 1 moraine looking upglacier, (g) the Khumbu 2 moraine looking upglacier, (h) the boulder from which sample KH1 was collected, (i) the Lobuche 3 moraine looking upglacier, (j) the boulder from which sample LB11 was collected. Note people and tents circled in red for scale.
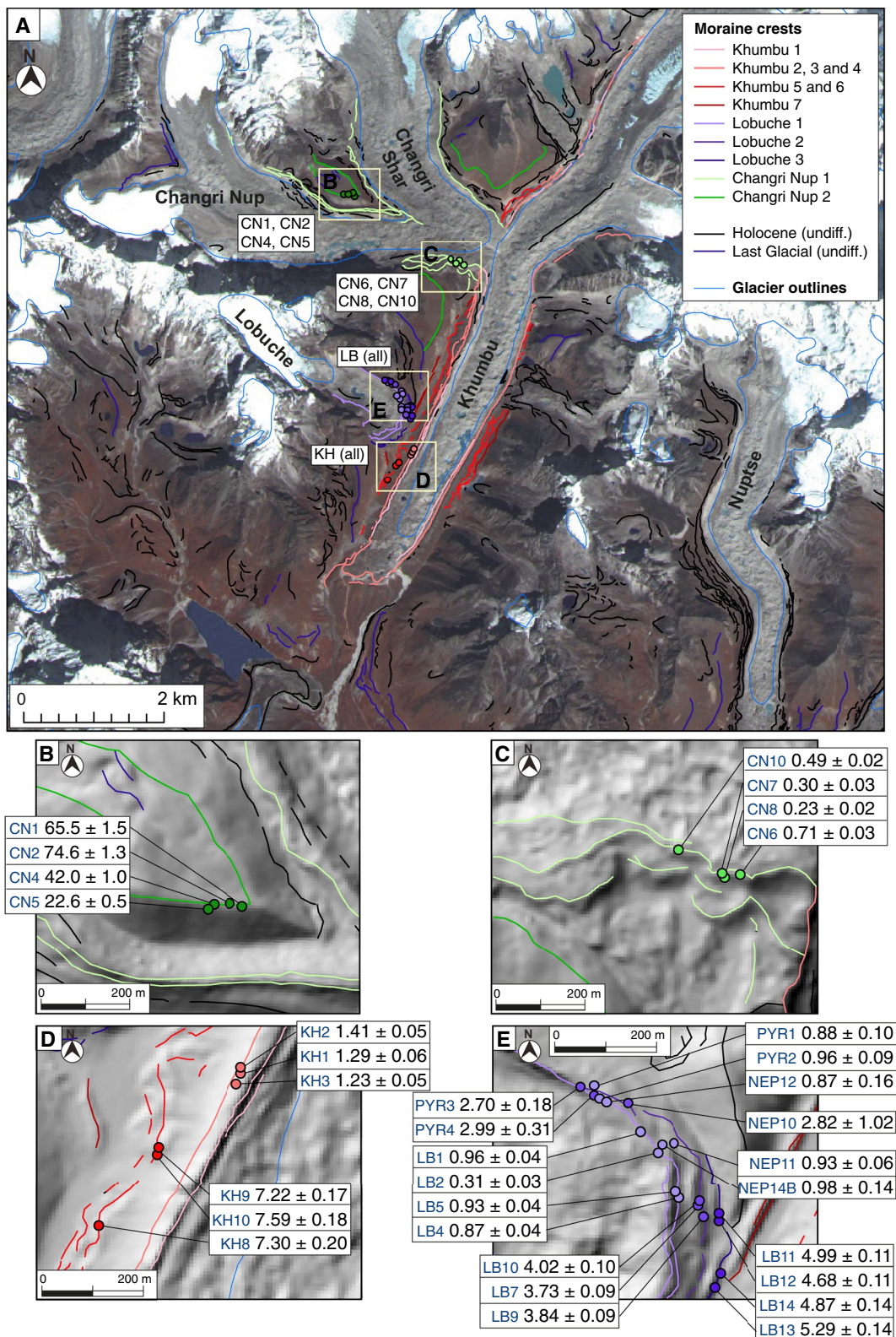
Figure 3. Map of moraine crests in the Khumbu Valley and sample locations where (a) shows an overview of the Khumbu Valley and locations of the sampled boulders for each glacier, with detail of sample locations for (b and c) Changri Nup Glacier moraines, (d) Khumbu Glacier moraines, and (e) Lobuche Glacier moraines. Glacier outlines are from the Randolph Glacier Inventory (RGI Consortium, 2017). Topographic imagery is from Landsat bands 7, 5, and 4 in 2015. Moraine crests are indicated by colored lines, where those that are not differentiated into detailed glacial stages are assigned as either Holocene or Late Glacial.

Table 1
Sample Description and Be-10/Be-9 Measurement Data, With Ages Calculated Using the Online Cosmogenic Nuclide Exposure-Age Calculator v.3 (Balco et al., 2008) Using a Global Production Rate (Borchers et al., 2016) and the Time Dependent Scaling Method of Lifton et al. (2014)

Moraine	Sample ID	Latitude (dd)	Longitude (dd)	Elevation (m a.s.l.)	Boulder size (m) a-axis	b-axis	c-axis	Sample thickness (cm)	Shielding correction	Quartz mass (g)
Khumbu 2	KH1	27.9487	86.8151	4,974	3.1	2.2	1.0	1.9	0.989	18.74
	KH2	27.9488	86.8151	4,974	4.1	2.4	1.6	2.9	0.989	20.41
	KH3	27.9485	86.8150	4,974	6.5	5.7	3.0	2.0	0.989	14.78
Khumbu 6	KH8	27.9451	86.8113	4,920	2.2	1.6	0.8	1.7	0.988	17.57
	KH9	27.9469	86.8128	4,938	4.6	3.1	2.2	1.9	0.988	20.77
	KH10	27.9469	86.8128	4,938	2.5	1.7	0.9	2.7	0.989	20.00
Changri Nup 1	CN6	27.9680	86.8228	5,084	2.6	1.8	1.5	2.4	0.990	17.12
	CN7	27.9730	86.8226	5,293	1.7	1.7	1.2	2.0	0.993	20.81
	CN8	27.9730	86.8226	5,295	3.8	2.6	1.6	2.4	0.993	20.27
	CN10	27.9737	86.8214	5,201	2.6	2.5	1.6	1.0	0.993	19.84
Changri Nup 2	CN1	27.9823	86.8067	5,314	2.7	2.0	1.1	2.4	0.994	18.83
	CN2	27.9824	86.8064	5,324	3.0	1.3	1.1	2.7	0.994	18.92
	CN4	27.9823	86.8059	5,329	2.1	1.3	0.8	2.6	0.994	20.71
	CN5	27.9822	86.8058	5,326	2.9	2.7	1.1	1.8	0.994	18.78
Lobuche 1	LB1	27.9565	86.8125	5,018	4.4	2.9	2.4	2.4	0.983	19.20
	LB2	27.9561	86.8129	5,012	3.5	3.2	2.4	2.8	0.984	18.11
	LB4	27.9551	86.8135	5,009	2.3	2.2	1.2	2.9	0.986	19.38
	LB5	27.9552	86.8134	5,012	3.7	2.6	2.1	4.3	0.986	18.85
	PYR1	27.9576	86.8113	5,016	2.2	1.5	1.1	3.0	0.960	23.15
	PYR2	27.9573	86.8114	5,023	1.6	0.7	0.7	3.0	0.960	28.92
	NEP14B	27.9562	86.8131	5,017	1.5	1.0	0.9	2.0	0.984	14.11
	NEP11	27.9562	86.8136	5,015	1.7	1.2	1.0	3.5	0.910	26.40
	NEP12	27.9573	86.8115	5,020	3.3	2.6	0.7	3.5	0.988	19.32
Lobuche 2	LB7	27.9548	86.8140	4,997	1.4	1.3	1.0	3.3	0.986	19.57
	LB9	27.9546	86.8141	4,995	2.0	0.9	0.8	2.3	0.986	19.46
	LB10	27.9549	86.8140	4,998	5.0	4.1	3.4	1.9	0.986	19.48
	PYR3	27.9576	86.8108	5,023	1.1	0.8	0.6	3.0	0.983	14.43
	PYR4	27.9573	86.8113	5,022	0.8	0.6	0.5	3.0	0.960	36.07
	NEP10	27.9572	86.8122	5,003	2.4	1.8	0.7	3.5	0.988	18.87
Lobuche 3	LB11	27.9546	86.8146	4,986	3.2	2.8	1.5	2.8	0.986	17.23
	LB12	27.9546	86.8146	4,985	2.6	2.1	1.3	1.6	0.986	19.62
	LB13	27.9530	86.8145	4,970	3.6	3.6	2.3	3.0	0.987	18.81
	LB14	27.9533	86.8147	4,970	4.3	3.8	3.8	1.9	0.987	19.13
	CB221019 (blank)									231.69
	CB270220 (blank)									240.95
	MBL02 (blank)									535.8
	VJB7 (blank)									159.9
	BKVR07 (blank)									203.8

Note. Ages are reported with their internal uncertainties. Be-10/Be-9 measurements for blanks used to calculate the internal uncertainties are reported below the table.

Be-9 added (μg)	Be-9 added uncertainty (μg)	Be-10/Be-9	Be-10/Be-9 uncertainty	Blank used	Be-10 (atoms g^{-1})	Be-10 uncertainty (atoms g^{-1})	Age (ka)	Internal uncertainty (ka)
230.16	3.25	9.15E−14	3.55E−15	CB221019	73,400	3,200	1.29	0.06
231.78	3.28	1.07E−13	3.33E−15	CB221019	79,500	2,900	1.41	0.05
230.25	3.26	6.89E−14	2.32E−15	CB221019	69,500	2,800	1.23	0.05
232.37	3.29	4.68E−13	1.01E−14	CB221019	411,000	11,000	7.30	0.20
231.86	3.28	5.47E−13	9.79E−15	CB221019	406,300	9,300	7.22	0.17
231.95	3.28	5.60E−13	1.03E−14	CB221019	433,000	10,000	7.59	0.18
246.46	3.48	4.05E−14	1.52E−15	CB270220	36,800	1,700	0.71	0.03
227.70	3.22	2.48E−14	1.61E−15	CB221019	16,600	1,400	0.30	0.03
230.76	3.26	1.86E−14	1.29E−15	CB221019	12,500	1,200	0.23	0.02
241.54	3.41	3.48E−14	1.40E−15	CB270220	26,400	1,300	0.49	0.02
231.18	3.27	6.88E−12	1.24E−13	CB221019	5,650,000	130,000	65.52	1.53
242.90	3.43	7.42E−12	7.57E−14	CB270220	6,370,000	110,000	74.56	1.31
225.32	3.19	5.21E−12	9.58E−14	CB221019	3,782,000	88,000	42.04	0.99
229.48	3.24	2.32E−12	4.40E−14	CB221019	1,893,000	45,000	22.58	0.54
240.10	3.39	6.30E−14	2.18E−15	CB270220	50,700	2,100	0.96	0.04
239.59	3.39	1.90E−14	1.21E−15	CB270220	14,700	1,300	0.31	0.03
240.52	3.40	5.58E−14	1.82E−15	CB270220	44,300	1,800	0.87	0.04
241.12	3.41	5.78E−14	1.92E−15	CB270220	47,400	1,900	0.93	0.04
156.6	0.62	3.50E−14	3.59E−15	VJB7	43,810	5,144	0.88	0.10
115.1	0.46	6.51E−14	5.48E−15	VJB7	49,064	4,569	0.96	0.09
155.3	0.62	2.56E−14	3.42E−15	BKVR07	52,091	7,650	0.98	0.14
158.7	0.63	3.86E−14	2.40E−15	BKVR07	44,284	2,986	0.93	0.06
500.5	2.50	3.14E−14	4.86E−15	MBL02	44,497	8,289	0.87	0.16
243.92	3.45	2.38E−13	4.23E−15	CB270220	196,600	4,500	3.73	0.09
239.59	3.39	2.51E−13	4.78E−15	CB270220	204,500	4,900	3.84	0.09
240.52	3.40	2.64E−13	5.05E−15	CB270220	216,000	5,200	4.02	0.10
500.2	2.50	6.85E−14	4.18E−15	MBL02	143,721	9,546	2.70	0.18
156.3	0.62	1.80E−13	1.83E−14	VJB7	155,550	16,032	2.99	0.31
488.1	2.44	9.30E−14	3.17E−14	MBL02	148,444	53,642	2.82	1.02
242.30	3.42	2.85E−13	4.44E−15	CB270220	265,500	5,700	4.99	0.11
241.96	3.42	3.09E−13	7.60E−15	CB270220	253,000	7,200	4.68	0.13
245.87	3.48	3.23E−13	7.02E−15	CB270220	280,200	7,300	5.29	0.14
241.37	3.41	3.11E−13	7.66E−15	CB270220	259,800	7,500	4.87	0.14
3.28	2.12E−15	9.45E−16						
3.41	2.36E−15	7.26E−16						
2.67	4.72E−15	4.71E−16						
0.63	2.97E−15	1.08E−15						
0.81	5.21E−15	1.15E−15						

were collected from boulders on the crest of the Khumbu 2 lateral moraine at a mean elevation of 4,974 m a.s.l. close to the terminal moraine of Lobuche Glacier (Figure 3d) to give an exposure age of 1.31 ± 0.1 ka.

The Khumbu 2 lateral moraine forms the highest crest above a more complex distal slope superimposed upon the Khumbu 6 moraine (Figure 2c). For 1 km downglacier of the palaeoconfluence with Changri Nup Glacier, the lateral moraine has a complex structure with multiple overlapping moraine lobes and ridge crests (Figure 4a). Geomorphological mapping revealed a divergence between the Khumbu 2 and Khumbu 6 moraines and the presence of deposits representing the Khumbu 3, Khumbu 4 and Khumbu 5 moraines; these moraines have no visible equivalent further downglacier where they are buried under the Khumbu 2 moraine (Figure 6). Upglacier from the palaeoconfluence, the Khumbu 3–5 moraines reappear and continue for about 1.2 km where they have been disturbed by large-scale slumping and were not sampled (Figure 3a).

The Khumbu 6 lateral moraine has multiple discontinuous crests and extends from 1.2 km upglacier of the terminus to the Changri Nup palaeoconfluence. The crest is rounded and has a relief of about 20 m above the valley floor. Three samples (KH8, KH9, and KH10) were collected from boulders on the crest of the true right Khumbu 6 lateral moraine at a mean elevation of 4,932 m a.s.l. downglacier of the section where the Khumbu 3–5 moraines are visible (Figure 3d) to give an exposure age of 7.37 ± 0.20 ka.

The Khumbu 7 lateral moraine is about 50 m wide and 15–20 m in relief, extending 1 km upglacier from the northern edge of the Lobuche terminal moraine (Figures 3a and 4a). This moraine was not sampled for exposure-age dating but based on its position is older than the Khumbu 6 moraine and therefore is early Holocene in age (older than 7.4 ka).

4.2. Changri Nup Glacier Moraines and Geochronology

Changri Nup and Changri Shar Glaciers have two sets of closely spaced moraines with distinct crests and asymmetrical slopes (Figures 2d and 2e). The moraines were identified on both sides of Changri Nup Glacier and along the topographic high marking the confluence with Changri Shar Glacier (Figures 3a and 4b).

The Changri Nup 1 moraine is 100 m in relief ranging in elevation from 5,110 to 5,401 m a.s.l., and continuous along the true left of Changri Nup Glacier from the convergence of the two glaciers to about 2.1 km upglacier. The Changri Nup 1 moraine is less distinct on the true right of the glacier where it is obscured by mass movement. Distinct crests extend 1.3 km upglacier from the former confluence with Khumbu Glacier with 50–70 m relief above the debris-covered former glacier surface. Four samples (CH6, CH7, CH8, and CH10) were collected from boulders with a mean elevation of 5,218 m a.s.l. (Figure 3b). A chi-squared test separated these samples into two pairs, with CN6 and CN10 giving an exposure age of 0.60 ± 0.16 ka, and CN7 and CN8 giving an exposure age of 0.26 ± 0.05 ka.

The Changri Nup 2 moraine is up to 300 m wide and 1.8 km long with a distinct crest ranging in elevation from 5,289 m to 5,443 m a.s.l. and proximal slopes inclined at 20°–38°. The Changri Nup 2 moraine is more vegetated than the Changri Nup 1 moraine with 70–80 m of relief from the base of the lateral morainic trough between these landforms. Four samples (CN1, CN2, CN4, and CN5) were collected from boulders at a mean elevation of 5,323 m a.s.l. (Figure 3c) with exposure ages ranging from 22.6 ± 0.5 to 74.6 ± 1.3 ka. As discussed in Section 5.2, we consider that the ages from this moraine are affected by inheritance of Be-10 prior to deposition in their sampled location.

4.3. Lobuche Glacier Moraines and Geochronology

Lobuche Glacier is surrounded by three compound ice-marginal moraines about 100 m wide, the Lobuche 1–3 moraines, bordering ice-cored moraine representing the former debris-covered tongue (Figures 3 and 4c) and indicating when Lobuche Glacier was confluent with Khumbu Glacier (Figure 2c). The closely spaced moraine crests are similar in elevation to the Khumbu 2 moraine and decrease in relief by about 100 m between the proximal and the distal crest. The Lobuche 2 and Lobuche 3 moraines are more rounded and vegetated than the Lobuche 1 moraine.
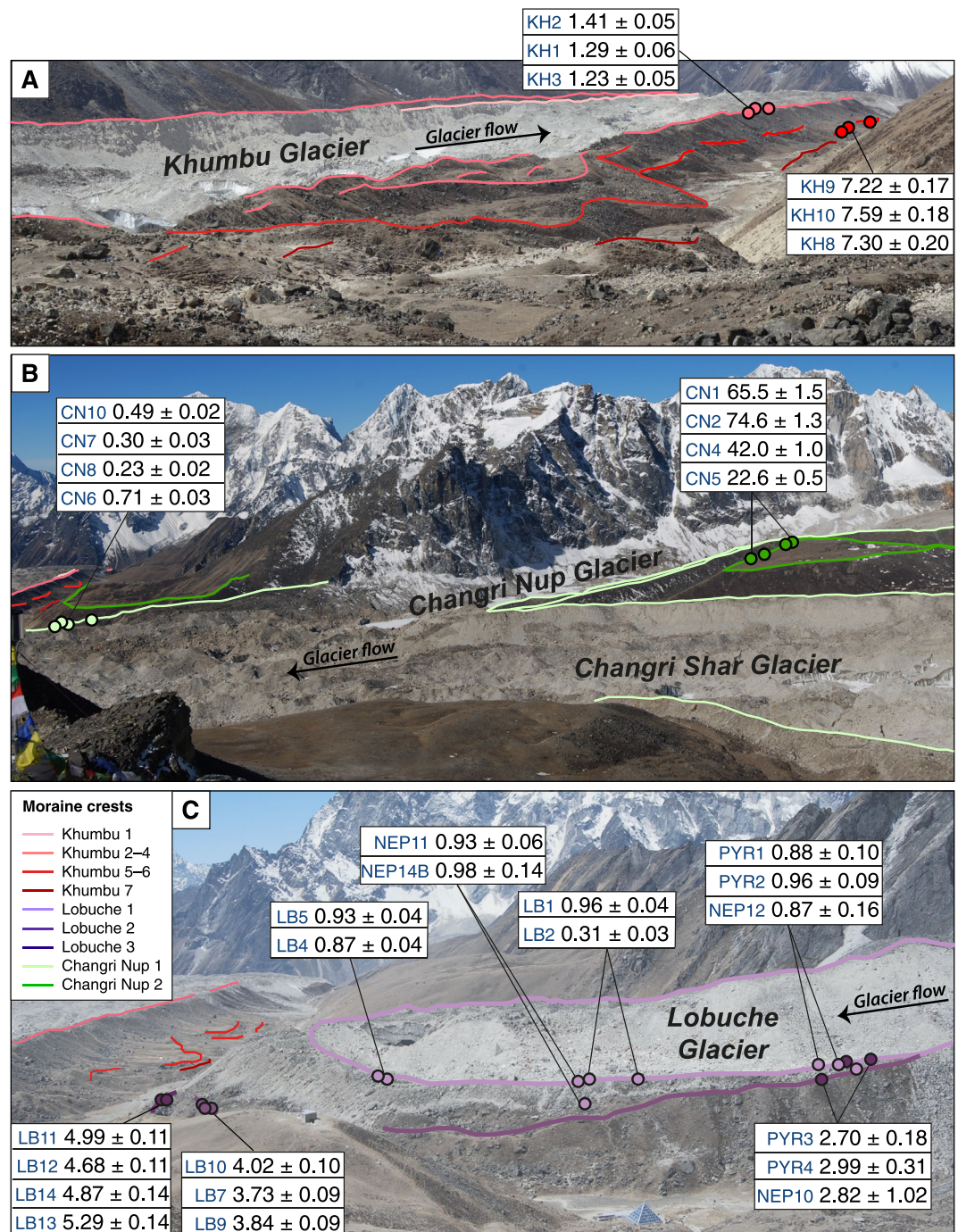
Figure 4. Perspective photographs of the moraines from which samples were collected for Be-10 exposure-age dating and the ages produced for each sample for (a) Khumbu Glacier, (b) Changri Nup Glacier, and (c) Lobuche Glacier. Note that the photograph of Khumbu Glacier shows the true right lateral moraines in the foreground where the complete sequence of seven moraines below the Changri Nup palaeoconfluence merges into three moraines further down-glacier. This section is shown in detail in Figure 6.

The Lobuche 1 moraine is the proximal crest that ranges from 5,009 m to 5,023 m a.s.l., reaching 80 m above the valley floor and 30 m above the former glacier surface. The sharp-crested moraine was traced from the terminus through the lateral moraines to where they merge into the valley sides (Figure 4c). Nine samples (LB1, LB2, LB4, LB5, PYR1, PYR2, NEP11, NEP12, and NEP14B) were collected from boulders with a mean elevation

of 5,016 m a.s.l. (Figure 3e) and a chi-squared test identified LB2 as an outlier. The exposure age based on the remaining eight samples is 0.92 ± 0.02 ka.

The Lobuche 2 moraine ranges from 4,930 to 5,010 m a.s.l. and is 55 m in relief. Six samples (LB7, LB9, LB10, PYR3, PYR4, and NEP10) were collected from boulders with a mean elevation of 5,006 m a.s.l. (Figure 3e). A chi-squared test identified two statistically distinct clusters of three samples, to give two ages for this moraine with 90% confidence intervals of 2.78 ± 0.15 ka (Lobuche 2A) and 3.85 ± 0.05 ka (Lobuche 2B).

The Lobuche 3 moraine ranges from 4,921 to 4,950 m a.s.l. and is 35 m in relief. Four samples (LB11, LB12, LB13, and LB14) were collected from boulders with a mean elevation of 4,978 m a.s.l. (Figure 3e) to give an exposure age of 4.96 ± 0.26 ka.

5. Discussion

5.1. Uncertainties Associated With Moraine Exposure Ages

Moraine exposure ages are subject to internal uncertainties arising from the measurement of Be-10 that are consistently low in our study, and systematic external uncertainties associated with the cosmogenic nuclide production rate and scaling. There is no production rate scaling method specific to Asia and therefore we used the global production rate scaling of Borchers et al. (2016). We assume that all the ages produced in this study and from Finkel et al. (2003) are subject to the same Be-10 production rate due to their location within one valley and compared these datasets using their internal uncertainties. When comparing the moraine exposure ages for the Khumbu Valley with those for regional glacial stages for the monsoon-influenced Himalaya in Section 5.3, we use their external uncertainties to account for regional variation in the Be-10 production rate. The Finkel et al. (2003) geochronology was recalibrated using the most recently updated production rate and a chi-squared test following the same approach as for the samples measured in this study, such that the Holocene moraine ages were 25%–31% older and the pre-Holocene ages were 4%–13% older.

Moraine exposure ages are subject to uncertainties arising from the geomorphological context of the sample (Kirkbride & Winkler, 2012); for example, if the boulder has been exposed prior to deposition in the sampled location. In Section 3.2, we addressed each of these potential sources of geomorphological uncertainty and conclude that our moraine exposure ages have not been significantly affected by past variations in vegetation, snow cover, or erosion of the boulder surfaces, that the lithology of the sampled boulders does not introduce an uncertainty to the exposure ages, and that shielding of the sampled boulder by the surrounding topography has been accurately constrained. The close clustering of the exposure ages for the Holocene moraines implies limited or no inheritance of Be-10. The wide distribution of ages for the Changri Nup 2 moraine is likely to result from inheritance of Be-10 during exposure prior to deposition in the sampled location. The accumulation of Be-10 during supraglacial transport depends on the rate of ice motion, and was minimal at Chhota Shigri Glacier in the Indian Himalaya (Scherler & Egholm, 2020). For Rongbuk Glacier, adjacent to the northern headwall of Khumbu Glacier, the exposure ages of three supraglacial boulders were 0.1–0.4 ka (Owen et al., 2009).

5.2. Interpretation of Individual Moraines

The Changri Nup 2 moraine represents a maximum extent of the upper ablation area of Khumbu Glacier. A chi-squared test identified samples CN4 and CN5 as similar at a 95% confidence interval, which would give a landform age of 70.0 ± 6.4 ka. However, while the scatter of the individual ages for the Changri Nup 2 moraine is large, ranging from 22.6 ± 1.4 to 74.6 ± 4.7 ka across four samples (Figure 5c), the internal uncertainties for each age are similar to those for the other samples in this study and therefore likely to represent inheritance of Be-10 from earlier exposure prior to moraine formation. The Changri Nup 2 moraine is located close to the Himalayan Main Divide, indicating that LGM moraines may survive in protected localities even in the highest valleys.

The Khumbu 6 moraine age does not correlate with the moraines formed by Lobuche Glacier (Figure 5a). Close to the Changri Nup palaeoconfluence, the lateral moraine of Khumbu Glacier forms a set of overlapping lobate moraines of a different form to the approximately parallel Khumbu 2 and Khumbu 6 moraine crests to the south (Figure 6a). Two well-developed lateral moraines and one smaller lateral moraine lie between the Khumbu 2 and Khumbu 6 moraines and each moraine overlaps the older landforms. This site reveals five moraine overtopping
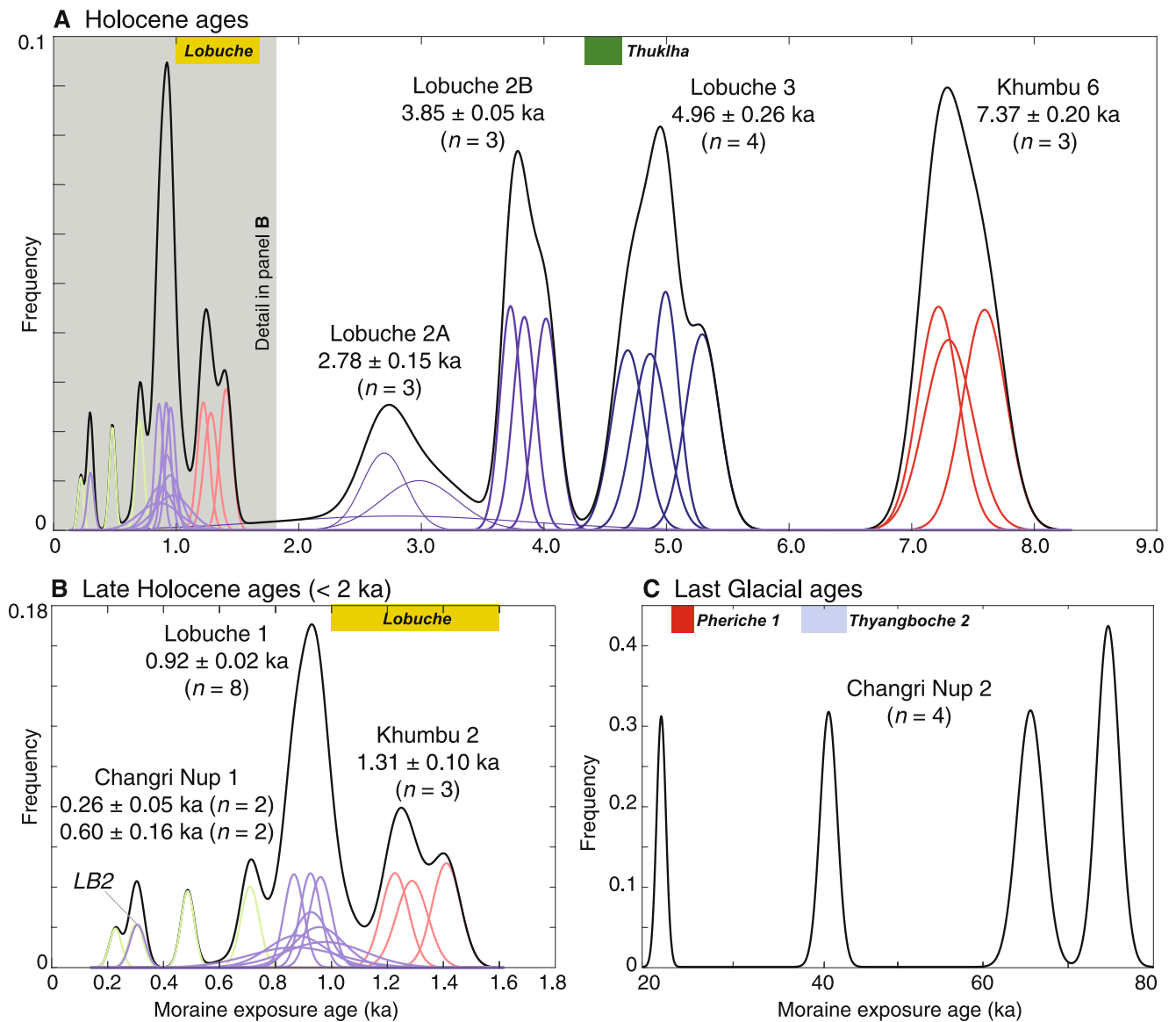
Figure 5. Normalized kernel age density plots for moraines surrounding Khumbu Glacier, Changri Nup Glacier, and Lobuche Glacier where (a) shows the Holocene geochronology, (b) shows moraine ages less than 2 ka with one sample (LB2) identified as an outlier that is shown but not used for calculation of the moraine age, and (c) shows Last Glacial ages from the Changri Nup 2 moraine. The bars show the local glacial stages identified by Finkel et al. (2003).

events of which the youngest (Khumbu 2; 1.3 ± 0.1 ka) and oldest (Khumbu 6; 7.4 ± 0.2 ka) bracket the ages of the intervening three undated moraines. The Khumbu 2 moraine is older than the Lobuche 1 moraine.

Lobuche Glacier is the only location where both terminal and lateral moraines were sampled. The exposure ages revealed four distinct periods of moraine building from three moraine crests; Lobuche 1 (0.9 ± 0.02 ka), Lobuche 2A (2.8 ± 0.2 ka), Lobuche 2B (3.9 ± 0.1 ka), and Lobuche 3 (5.0 ± 0.3 ka). The two ages for the Lobuche 2 moraine are significantly different and suggest that the terminal section is older than the lateral sections. The timing of moraine formation may therefore have been time-transgressive, with the lateral moraine being overtopped by a later phase of glacier expansion, implying that the moraine crest is a palimpsest feature.

5.3. Interpretation of Moraine Ages in the Context of Regional Glacial Stages

Exposure-age dating of moraines is widely used across High Mountain Asia to determine the timing and duration of regional glacial stages (e.g., Owen & Dortch, 2014; Saha et al., 2018, 2019; Solomina et al., 2015). We
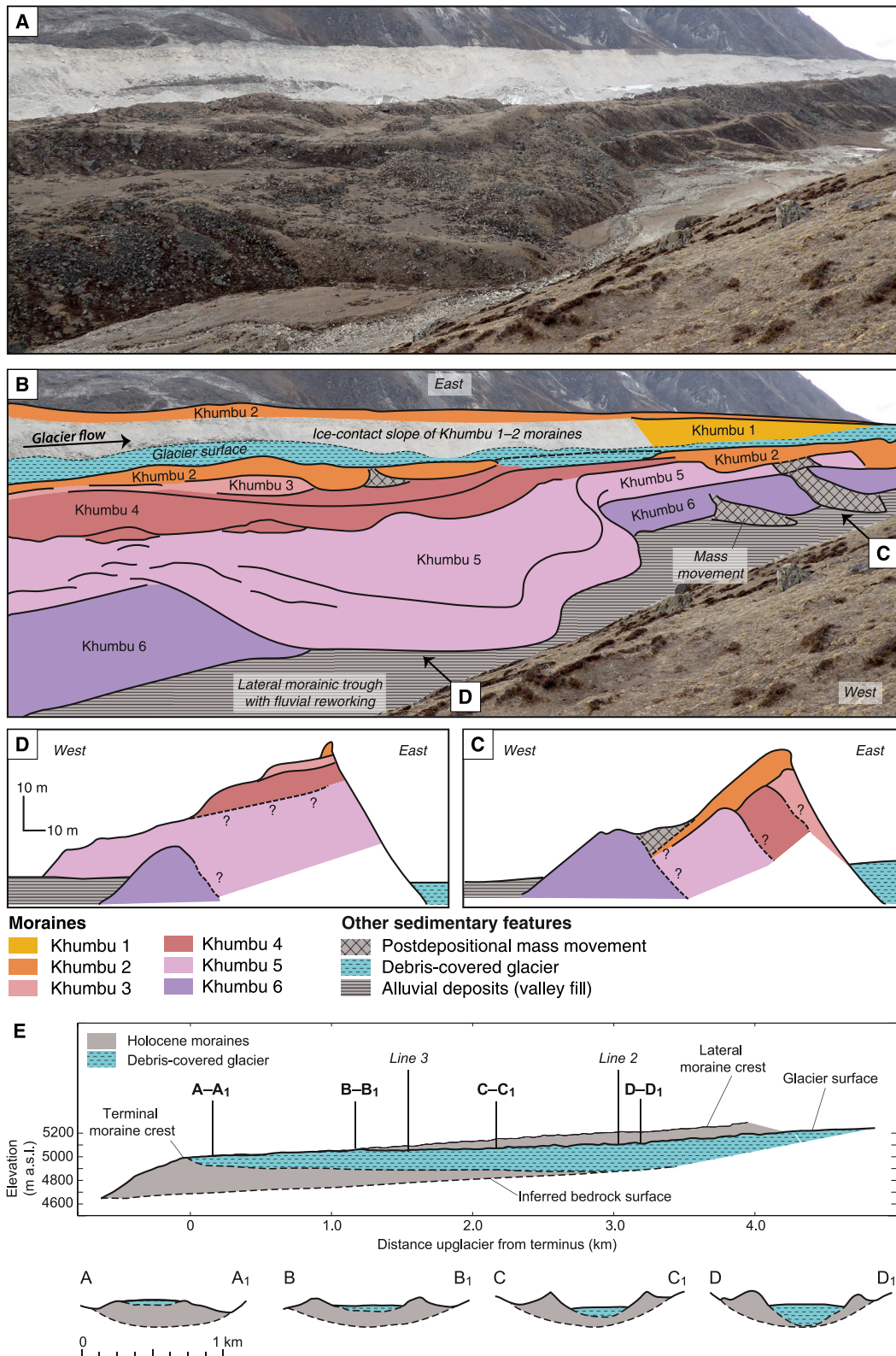
Figure 6.

Table 2
Correlation of Moraine Ages Produced in This Study With Glacial Stages Identified the Upper Khumbu Valley by Finkel et al. (2003) and the Regional Glacial Stages Identified for the Monsoon-Influenced Himalaya (MOHITS) by Murari et al. (2014)

Khumbu Valley moraine name	Correlative moraine	Local moraine age (ka)	Khumbu Valley glacial stage (Finkel et al., 2003)	MOHITS regional glacial stages (Murari et al., 2014) Name	Age (ka)
Changri Nup 1	Khumbu 1?	0.60 ± 0.16	–	MOHITS 1A	0.4 ± 0.1
Lobuche 1	–	0.92 ± 0.06	–	MOHITS 1B	0.7 ± 0.1
Khumbu 2	–	1.31 ± 0.12	Lobuche (1.3 ± 0.31)	MOHITS 1C	1.5 ± 0.2
Khumbu 3	**Lobuche 2A**	2.78 ± 0.22	Lobuche (1.3 ± 0.31)	MOHITS 1D	2.3 ± 0.1
Khumbu 4	**Lobuche 2B**	3.85 ± 0.23	–	MOHITS 1E	3.5 ± 0.4
Khumbu 5	**Lobuche 3**	4.96 ± 0.39	Thuklha (4.5 ± 0.30)	MOHITS 1F	5.4 ± 0.6
Khumbu 6	–	7.37 ± 0.45	–	MOHITS 1G	7.7 ± 0.6
–	–	–	–	MOHITS 1H	8.1 ± 0.8
–	–	–	–	MOHITS 1I	9.1 ± 0.3
–	–	–	–	MOHITS 1J	10.1 ± 0.8
Khumbu 7	–	11.5 ± 0.70	Chhukung (11.5 ± 0.70)	MOHITS 1K	11.4 ± 0.7
–	–	–	–	MOHITS 2A	12.9 ± 0.9
–	–	–	–	MOHITS 2B	15.5 ± 1.3
–	–	–	–	MOHITS 2C	17.3 ± 0.3
Pheriche 2	–	17.1 ± 1.0	Pheriche 2 (17.1 ± 1.0)	MOHITS 2D	18.7 ± 1.8
Changri Nup 2	Pheriche 1	22.6 ± 1.4 (n = 1)	Pheriche 1 (24.4 ± 1.2)	MOHITS 2E	22.0 ± 2.0

Note. The external uncertainties associated with each moraine age are used here to enable a regional comparison. The moraines dated in this study are in bold text. Ages in italic text are recalibrated from Finkel et al. (2003). Note that the Changri Nup 2 moraine age is given as the youngest sample age for this moraine.

compared our results from the upper Khumbu Valley with a regional moraine geochronology that identified 11 Holocene glacial stages (Table 2; Murari et al., 2014). To account for regional variation in the Be-10 production rate, we compared the geochronology for the Khumbu Valley to that for the monsoon-influenced Himalaya using the external uncertainties associated with each moraine age.

The regional LGM was dated to 22 ± 2 ka (MOHITS 2E) and correlates to Marine Isotope Stage 2 and the global LGM (Murari et al., 2014). This stage is similar in age to the youngest sample from the Changri Nup 2 moraine (22.6 ± 1.4 ka) and the Pheriche 1 moraine (24.4 ± 2.2 ka) identified by Finkel et al. (2003). The four oldest Holocene MOHITS stages were dated to 11.4 ± 0.7, 10.1 ± 0.5, 9.1 ± 0.3, and 8.1 ± 0.8 ka (MOHITS 1K–1H). The oldest of these stages is similar in age to the Chhukung stage (11.5 ± 0.7 ka) in the Khumbu Valley (Figure 1, Table 2) and to the ages of three OSL samples collected from glacier-associated sediments, one of which was collected from a supraglacial sand deposit within the terminal moraine of Khumbu Glacier (Figure 1; Richards et al., 2000).

Seven of the regional Holocene glacial stages (MOHITS 1G–1A) are represented by the Khumbu and Lobuche Glacier moraines (Table 2). There are two events within the Holocene Climatic Optimum: the Khumbu 6 moraine

Figure 6. Interpretation of the lateral moraine sequence on the true right (west) of Khumbu Glacier immediately below the palaeoconfluence with Changri Nup Glacier, and the Holocene moraine volume. (a) Photograph of the lateral moraines looking eastwards toward Khumbu Glacier from the Last Glacial lateral moraine. (b) Geomorphological interpretation of the moraines shown in (a). The schematic cross-sections (c and d) are drawn with a vertical exaggeration of 1.5 to show (c) where only the Khumbu 2 and Khumbu 6 moraines are visible at the surface, and (d) further upglacier where the complete sequence of Khumbu moraines are visible. The question marks indicate the inferred contacts between different moraines in the subsurface. The Khumbu 2 moraines are about 40–50 m in relief above the valley floor and the entire landform is about 200 m in width. (e) Estimation of Holocene moraine volume in the lower ablation area of Khumbu Glacier showing the long-profile sections estimated from observations of the position of the glacier bed and extrapolated from radio echo-sounding surveys (indicated by Line 3 and Line 2; Gades et al., 2000), and the estimated sediment area at four cross-sections through the long profile, indicated as A–D. These measurements were used to calculate the total sediment volume and to infer catchment denudation rate, as described in the Supporting Information S1.

(7.4 ± 0.4 ka) correlates to the MOHITS 1G stage (7.7 ± 0.6 ka) and the Lobuche 3 moraine age (5.0 ± 0.4 ka) correlates to the MOHITS 1F stage (5.4 ± 0.6 ka), which is similar to the Thuklha stage (4.5 ± 0.3 ka). There are three events within the Roman humid period: Lobuche 2B (3.9 ± 0.2 ka) correlates to the MOHITS 1E stage (3.5 ± 0.4 ka) and Lobuche 2A (2.8 ± 0.2 ka) is slightly older than the MOHITS 1D stage (2.3 ± 0.1 ka). The Khumbu 2 moraine (1.3 ± 0.1 ka) correlates to the MOHITS 1C stage (1.5 ± 0.2 ka) and the Lobuche stage (1.3 ± 0.3 ka). There is one event within the Medieval Warm Period: the Lobuche 1 moraine (0.9 ± 0.05 ka) is slightly older than the MOHITS 1B stage (0.7 ± 0.1 ka). The Changri Nup 1 moraine (0.60 ± 0.16 ka) correlates to the MOHITS 1A stage (0.4 ± 0.1 ka) and the Little Ice Age (LIA) maximum (Murari et al., 2014; Rowan, 2017). C-14 dating of glacier-associated landforms in the Khumbu Valley gave ages between 1.49 ± 0.2 and 0.34 ± 0.2 ka from 21 samples (summarized in Rowan, 2017) supporting the interpretation that this was an active phase of moraine building. The Khumbu 1 moraine is morphostratigraphically consistent with the Changri Nup 1 moraine and its age could therefore be equivalent to the LIA.

Finkel et al. (2003) suggested two phases of glacier expansion during the Lobuche stage in the upper Khumbu Valley: one representing the late Roman humid period and one the LIA maximum, with a combined age of 1.3 ± 0.3 ka (Figure 1). Applying a chi-squared test to their five samples separates the ages into the Lobuche stage (1.3 ± 0.3 ka; $n = 3$) and a historical event (0.10 ± 0.03 ka; $n = 2$). The older stage is similar to the Khumbu 2 moraine and MOHITS 1C, while the younger event could indicate the end of the LIA or later reworking of the moraine surface. Two of the three Be-10 ages used to define the Lobuche stage were from moraines in the Chhukung Valley and one from the terminal moraine of Khumbu Glacier, with a similar OSL age from the outwash deposits at Lhotse Nup Glacier.

The Lobuche 1 moraine age is unlikely to be affected by inheritance from supraglacial transport as the duration of ice flow through this small, steep glacier would be shorter than for the Rongbuk Glacier (see Section 5.1), and therefore we expect this moraine to correlate to the MOHITS 1B stage even when geomorphological uncertainty is accounted for. The formation of the Changri Nup 1 moraine and the undated Khumbu 1 moraine were likely contemporaneous to the development of extensive supraglacial debris across Khumbu Glacier (Rowan et al., 2015). The debris mantle is unlikely to have extended upglacier of the Changri Nup 1 lateral moraine as this location in the upper ablation area was only subject to supraglacial debris transport over short distances. However, the Khumbu 1 lateral moraine formed in the lower ablation area and could have accumulated an inherited signal during supraglacial transport, such that the exposure age of this moraine may be up to 0.4 ka older than the Changri Nup 1 moraine. Alternatively, the dynamic response of Khumbu Glacier to late Holocene climate change could have resulted in a genuine difference in moraine ages based on their positions, as discussed in the following section.

5.4. Moraine Building as an Indicator of the Dynamic Response of Glaciers to Climate Change

Be-10 exposure ages identified eight periods of Holocene moraine crest aggradation in the upper Khumbu Valley (Table 2). Geomorphological mapping identified seven Holocene moraines formed by Khumbu Glacier (Figure 6) whereas only three equivalent landforms were identified for Lobuche Glacier. The composite Holocene moraine sequence in the upper Khumbu Valley appears to be coherent and complete (*sensu* Kirkbride & Winkler, 2012). We sampled the lateral moraines of Khumbu and Changri Nup Glaciers and the terminal and lateral moraines of Lobuche Glacier because glaciers transporting large volumes of sediment can become impounded by their moraines such that the terminal moraines may not be a reliable record of glacier change (Anderson et al., 2021; Rowan et al., 2022). However, placing our moraine geochronology in the context of regional glacial stages indicates that the timing of formation of the Last Glacial and Holocene moraines was unaffected by the influence of supraglacial debris on mass balance and ice flow. We infer that moraine building occurred largely by deposition of supraglacial debris in the early stages of overtopping of bounding moraine ridges as glaciers thickened, with limited accretion of basal till onto the proximal faces of the moraines. The glacier response times were shorter than the intervals of 0.6–2.0 kyr between phases of moraine construction (Table 2). The dynamic response time of Khumbu Glacier to the change in mean annual air temperature between the LIA and the present day was quantified using numerical modeling as 200–300 years (Rowan et al., 2021) and for Lobuche Glacier this will be shorter due to its relatively small size and steep slope (Oerlemans, 1989). Therefore, we suggest that the difference in the number of glacial stages represented at Khumbu and Lobuche Glaciers is the result of the superimposition of sediment that has buried some older moraine crests.

Undated Last Glacial stage moraines in the upper Khumbu Valley indicate that Lobuche Glacier converged with Khumbu Glacier during the LGM (Figure 3). The earliest Holocene moraine identified is the undated Khumbu 7 moraine that occupies the valley floor between Khumbu Glacier and Lobuche Glacier (Figure 3). This moraine formed prior to the deposition of the Khumbu 6 moraine and may be equivalent to the Chhukung stage (11.5 ± 0.2 ka). From the position of the Khumbu 7 moraine, we infer that Lobuche Glacier was not confluent with Khumbu Glacier during the early Holocene and has responded independently to climate change during this period. We therefore consider the Holocene moraine geochronologies as resulting from the response to the same change in climate of two distinct glaciers with differing geometries and dynamic behavior. The Khumbu 6 moraine has relatively low relief and its crest is more distal than the Khumbu 2 moraine, indicating that during the early Holocene the glacier surface was wider and at a lower elevation before multiple phases of moraine superposition built the crest represented by the Khumbu 2 moraine. This period of moraine building indicates a greater ice thickness during later expansion, as the glacier was unable to override or remove moraine barriers formed during previous advances. This resulted in the accumulation of a large volume of subglacial sediment that raised the glacier bed in the lower ablation area, as indicated by a pronounced reversal of bed slope in the subglacial long profile (Figure 6e).

5.5. Evolution of Khumbu Glacier From the LGM to the Late Holocene

The Last Glacial Khumbu Glacier formed the two Pheriche terminal moraines at 4,300 m a.s.l. during the global LGM and the local LGM (MOHITS 2E–2D), indicating that the glacier was 22.5 km long at the LGM. Lobuche and Changri Nup Glaciers were tributaries of Khumbu Glacier during the Last Glacial and the Changri Nup 2 lateral moraine formed during the global LGM in the upper ablation area of Khumbu Glacier. Regional Late Glacial stages (MOHITS 2C–2A) were not identified and glacier change in the Khumbu Valley during this period is unconstrained.

The early Holocene advance identified from the Chhukung stage lateral moraines (MOHITS 1K), assumed to include the Khumbu 7 lateral moraine, suggests that the terminus of Khumbu Glacier was in the upper part of the Pheriche Valley below Dughla Village at 4,400–4,500 m a.s.l. and that the glacier was about 18 km long (Figures 1 and 2b). Our estimate of subglacial sediment thickness suggests that the glacier rests on bedrock or a thin sediment layer upglacier of the Khumbu 7 moraine, and the position and low relief of this moraine indicates that the glacier tongue was narrower and thicker later in the Holocene, rather than that a similar ice thickness accommodated by a higher bed. Three subsequent early Holocene stages (MOHITS 1J–1H) were not identified.

During the mid-Holocene, the terminus of Khumbu Glacier was located around 4,900 m a.s.l. and the glacier was 16.5 ka long, similar to the present-day extent. Lobuche Glacier detached from Khumbu Glacier before 7.4 ka (MOHITS 1G) and formed the oldest (Lobuche 3) terminal moraine during the Thuklha stage (MOHITS 1F) which is also recorded by the Nuptse and Lhotse Nup Glacier moraines in the Chhukung Valley (Figure 1). During this time, Khumbu Glacier underwent a major shift in dynamic behavior, from responding to each glacial stage through a change in terminus position in the early Holocene to thickening of the ablation area to build a closely spaced set of moraines with increasing crest heights through subsequent glacial stages. This change in dynamic behavior suggests that Khumbu Glacier was unable to advance beyond the barrier created by the Khumbu 6 moraine, and therefore that mass gain was accommodated by thickening of the glacier tongue. The glacier overtopped the lateral moraines in the upper ablation area to form the Khumbu 5 moraine but did not expand sufficiently further downglacier to overtop moraines in the lower ablation area (Figures 6b–6d).

During the late Holocene, the terminus remained in a similar position at 4,900 m a.s.l. and the Khumbu 4 and Khumbu 3 moraines represent an increase in ice surface elevation without any widening during MOHITS 1E and 1D, suggesting a reduced ice flux from the Changri Nup and Changri Shar tributaries. Lobuche Glacier may have undergone a similar change in dynamic behavior as these two periods are represented by the Lobuche 2 moraine that yielded two distinct ages and could be interpreted as an initial expansion of the lower ablation area to build the terminal moraine followed by lateral expansion upglacier during the later glacial stage when the terminus was constrained (Figure 4c).

The last glacier expansion in the Khumbu Valley represented by the Khumbu 2 moraine occurred around 1.3 ka (MOHITS 1C) when the glacier surface overtopped the Khumbu 5–3 moraines in the lower ablation area without expanding beyond the Khumbu 6 moraine (Figure 6). This stage is represented in the Chhukung Valley, where

each of the five major glaciers built moraines contemporaneously with the Khumbu 2 moraine (Figure 1). This stage was not identified for Lobuche Glacier; the Lobuche 1 moraine may bury the equivalent to the Khumbu 2 moraine and is similar in age to MOHITS 1B.

The change in length of Khumbu Glacier between the LGM and the mid–late Holocene was 6.0 km (27% of the LGM glacier length) and equivalent to a change in ice surface elevation of 600 m. The length of Khumbu Glacier reduced by 4.5 km with a change in elevation of 100–200 m from the LGM to the early Holocene, then by 1.5 km with a change in elevation of 400–500 m from the early Holocene to the late Holocene around 8 ka when a change in dynamic behavior was initiated by the formation of large moraines that constrained subsequent ice margin fluctuations.

5.6. Estimated Holocene Catchment-Wide Denudation Rate

When the export of coarse sediment from a glacier is suppressed by the decoupling of the glacier from proglacial transport systems (Benn et al., 2003), englacial debris becomes trapped in ice-marginal and subglacial moraines and most of the sediment yield from the glacierized catchment is stored in raised-bed superposed moraine complexes (Lliboutry, 1986). Decoupled glacial-proglacial systems can be used to estimate the catchment denudation rate over timescales of 10^3 years if robust geochronological constraints on the accumulation of the moraine edifice are available. The catchment upvalley from the early Holocene terminal moraine drains the highest topography on Earth, and a multi-millennia denudation rate will integrate sediment yield by nival, periglacial and glacial erosion in this extreme environment.

Subglacial sediment volume can be predicted from a dimensionless index based on a ratio of catchment and glacier properties; primarily headwall height, slope and area (Maisch et al., 1999; Zemp et al., 2005). Low-gradient debris-covered glacier tongues in the Khumbu Valley are interpreted as having no erosional potential (Scherler et al., 2011) and, using the criteria of Maisch et al. (1999), Khumbu Glacier is likely to rest on a raised sediment bed. The geomorphology of the terminus supports this interpretation; for example, the main outwash stream does not incise through the moraine rampart (Figure 2b; Benn et al., 2003; Hambrey et al., 2008). The glacier bed long-profile shows a constant first-order down-valley slope of 0.03 between 3.2 and 8 km above the terminus (Figure 6e; Gades et al., 2000; Miles et al., 2018). At this point there is a pronounced break of slope and the bed slope reverses and rises toward the terminal moraine. This reversed bed slope is consistent with subglacial accretion of sediment to form a raised bed beneath the low-gradient, slow-moving glacier tongue. The break of slope is interpreted to mark the upper limit of a thick sediment bed. Be-10 exposure ages constrain the inception of the subglacial-ice-marginal moraine edifice to shortly before the crest age of the Khumbu 6 moraine—placing the main phase of Holocene moraine building within the last 8 ka.

The volume of the Holocene moraine complex was estimated by linear extrapolation of the bed long profile down-glacier from 3.2 km above the terminus, assuming that this represents the depth of the bedrock. The extrapolated bedrock surface was projected to emerge from beneath the terminal moraine ramp coincident with a pronounced break of slope at 4,620 m a.s.l. near Dughla (Figure 2b). A center-line profile and four cross-sections were constructed at 1 km intervals above the terminus and the moraine–bedrock contact was interpolated by extending the valley-side profiles as parabolic curves to intersect the extrapolated centerline of the bedrock surface. The upper cross-profile (D–D₁) is located at the upvalley edge of the reverse slope and lower cross-profile (A–A₁) is located close to the terminus (Figure 6e). The volume of the moraine complex was estimated as the mean cross-sectional area multiplied by the downvalley distance to the terminus and this was added to an estimate of the volume of the frontal sediment ramp based on the extrapolated rock bed (Supporting Information S1). Moraine volume was converted to whole rock volume using a void ratio of 0.3 (Conway & Rasmussen, 2000).

The estimated total moraine volume was 2.38×10^8 m³ representing a sediment yield of 1.82×10^3 kg km⁻² a⁻¹ assuming a rock density of 2.2×10^3 kg m⁻³, to give a catchment-averaged denudation rate of 0.8 mm a⁻¹ (Table S2 in Supporting Information S1). This value is a minimum estimate because; (a) we have not included the entire lateral moraine system, and (b) a minor fraction of the sediment yield is evacuated via proglacial streams as suspended sediment and during occasional outburst floods (Irvine-Fynn et al., 2017). To estimate the upper limit of the catchment-wide denudation rate, we included the lateral moraine volume upglacier of the break of slope at 3.2 km. We assumed a mean vertical height over the whole length of lateral moraines of either 50 or 100 m from the moraine crest to where the distal moraine slope meets the hillside over a distance of 10.8 km including the

Changri Nup moraines. We derived the cross-sectional area assuming that the proximal and distal moraine slopes form a right angle at the crest, using a distal slope of 38° and a proximal slope of 55° indicated from the DEM. The estimated lateral moraine volumes combined with that for the lower ablation area give a sediment yield of between 2.31×10^3 and 3.06×10^3 kg km^{-2} a^{-1} depending on the assumed lateral moraine relief, equivalent to a catchment-wide denudation rate of between 1.2 and 1.4 mm a^{-1}.

Several studies calculated Late Pleistocene denudation rates using Be-10 surface exposure to represent rockwall erosion over centennial to millennial timescales south of the Main Divide in the Central Himalaya, and generally show increasing denudation to the north, that is, with increasing elevation. Late Glacial (∼16 ka) denudation rates in the Yamuna Valley in northwest India were 1.9–3.0 mm a^{-1} and present-day values are similar (Kapannusch et al., 2020). Denudation rates are slightly lower in the Arun Valley in eastern Nepal (1.5 mm a^{-1}; Olen et al., 2015), at Chhota Shigri Valley in northwest India (0.6–1.3 mm a^{-1}; Scherler & Egholm, 2020) and at Milarepa's Glacier in central Nepal (1.2–1.3 mm a^{-1}; Heimsath & McGlynn, 2008). Catchment-wide denudation rates from 30 valleys in central Nepal are 2–3 mm a^{-1} (Godard et al., 2014). Last Glacial to late Holocene bedrock incision in the Khumbu Valley was previously estimated as 3.9 mm a^{-1} (Barnard et al., 2006); somewhat higher than the catchment-wide rates estimated here and by previous studies. Our Holocene catchment-wide denudation rate of 0.8–1.4 mm a^{-1} for the Khumbu Valley is similar to that estimated for much of the Central Himalaya close to the Main Divide. This estimate integrates short-term variations in erosion and sediment production over millennial timescales and the spatial integration of debris production by extra-glacial and subglacial erosion processes across the whole of the upstream catchment, comprising some of the highest-elevation topography on Earth.

6. Conclusions

The response of Himalayan glaciers to climate change is complicated by the influence of active tectonics and high-relief topography on ice flow and glacier mass balance. However, over millennial timescales, the timing of regional glacier change was broadly synchronous across the monsoon-influenced Central Himalaya. We present a geochronology for Holocene ice-marginal moraines in the upper Khumbu Valley in the Everest region of Nepal that constrains seven glacial stages between 7.4 ± 0.5 and 0.6 ± 0.2 ka. The deglaciation after the LGM is indicated by the local Pheriche 2 stage (17.1 ± 0.3 ka). The Post Glacial moraine record is incomplete but does indicate that glaciers in the Khumbu Valley generally receded until the local Chhukung stage (11.5 ± 0.2 ka) at the start of the Holocene. Eight of 11 regional stages Holocene glacial stages for the monsoon-influenced Himalaya are recorded by moraines in the Khumbu Valley, including the seven most recent stages identified in this study. The three Holocene glacial stages partially identified from the Khumbu Glacier moraines (Khumbu 5–Khumbu 3) and the two stages not identified from the Lobuche Glacier moraines (Khumbu 6 and Khumbu 2) are probably concealed within composite landforms where younger moraines were superimposed onto older ones. The identification of a complete sequence of seven regional glacial stages in the Khumbu Valley moraines indicates that high-elevation monsoon-influenced glaciers have responded consistently to regional climate change and that the moraines produced by such glaciers are useful indicators of their response to palaeoclimate change.

The Khumbu Glacier moraines indicate a change in glacier behavior during regional glacial stages after 8 ka: from advance and recession of the ice margin along and across valley to vertical expansion of the glacier surface. The ablation area of Khumbu Glacier has evolved from a wide, unconstrained ice tongue to a narrow, thick tongue due to repeated superposition of lateral and terminal moraines after 8 ka, represented by the increasing relief of five moraine crests (Khumbu 6–Khumbu 2). During the same period, the smaller, steeper Lobuche Glacier built a sequence of moraines that appears to represent three or four stages of glacier expansion (Lobuche 3–Lobuche 1) as Be-10 exposure ages suggest that the Lobuche 2 moraine may be a palimpsest feature representing two phases of glacier expansion.

While glaciers in the Central Himalaya may be expected to exhibit differences in behavior compared to those elsewhere in High Mountain Asia due to the influence of the Indian Summer Monsoon, regionally the moraines formed by these glaciers indicate a coherent response to Late Quaternary climate change. These results suggest that the moraines formed by monsoon-influenced glaciers in catchments with high-relief topography and high sediment yields can provide a complete and accurate record of regional palaeoclimate change when the differences in the processes by which individual glaciers form and preserve moraines are carefully considered.

Data Availability Statement

Sample data collected and measurements are available from the open access Informal Cosmogenic Nuclide Exposure-age Database (https://version2.ice-d.org/alpine/).

References

Anderson, L. S., & Anderson, R. S. (2018). Debris thickness patterns on debris-covered glaciers. *Geomorphology*, *311*, 1–12. https://doi.org/10.1016/j.geomorph.2018.03.014

Anderson, L. S., Armstrong, W. H., Anderson, R. S., & Buri, P. (2021). Debris cover and the thinning of Kennicott Glacier, Alaska: In situ measurements, automated ice cliff delineation and distributed melt estimates. *The Cryosphere*, *15*(1), 265–282. https://doi.org/10.5194/tc-15-265-2021

Aoki, T., & Imamura, M. (1999). Reconstructing the glacial chronology based on the ^{10}Be exposure age in the Khumbu Glacier, Eastern Nepal Himalaya. *Proceedings of the Korea-Japan/Japan-Korea Geomorphological Conference* (pp. 134–135).

Balco, G. (2011). Contributions and unrealized potential contributions of cosmogenic-nuclide exposure dating to glacier chronology, 1990–2010. *Quaternary Science Reviews*, *30*(1–2), 3–27. https://doi.org/10.1016/j.quascirev.2010.11.003

Balco, G. (2020). Glacier change and paleoclimate applications of cosmogenic-nuclide exposure dating. *Annual Review of Earth and Planetary Sciences*, *48*(1), 21–48. https://doi.org/10.1146/annurev-earth-081619-052609

Balco, G., Stone, J. O., Lifton, N. A., & Dunai, T. J. (2008). A complete and easily accessible means of calculating surface exposure ages or erosion rates from ^{10}Be and ^{26}Al measurements. *Quaternary Geochronology*, *3*, 174–195. https://doi.org/10.1016/j.quageo.2007.12.001

Barnard, P. L., Owen, L. A., & Finkel, R. C. (2006). Quaternary fans and terraces in the Khumbu Himal south of Mount Everest: Their characteristics, age and formation. *Journal of Geological Society*, *163*(2), 383–399. https://doi.org/10.1144/0016-764904-157

Benn, D. I., Bolch, T., Hands, K., Gulley, J., Luckman, A., Nicholson, L. I., et al. (2012). Response of debris-covered glaciers in the Mount Everest region to recent warming, and implications for outburst flood hazards. *Earth-Science Reviews*, *114*(1–2), 156–174. https://doi.org/10.1016/j.earscirev.2012.03.008

Benn, D. I., Kirkbride, M. P., Owen, L. A., & Brazier, V. (2003). Glaciated valley Landsystems. *Glacial Landsystems*, 372–406.

Borchers, B., Marrero, S., Balco, G., Caffee, M., Goehring, B., Lifton, N., et al. (2016). Geological calibration of spallation production rates in the CRONUS-Earth project. *Quaternary Geochronology*, *31*, 188–198. https://doi.org/10.1016/j.quageo.2015.01.009

Braucher, R., Guillou, V., Bourlès, D. L., Arnold, M., Aumaître, G., Keddadouche, K., & Nottoli, E. (2015). Preparation of ASTER in-house ^{10}Be/^{9}Be standard solutions. *Nuclear Instruments and Methods in Physics Research Section B: Beam Interactions with Materials and Atoms*, *361*, 335–340. https://doi.org/10.1016/j.nimb.2015.06.012

Braumann, S. M., Schaefer, J. M., Neuhuber, S. M., Lüthgens, C., Hidy, A. J., & Fiebig, M. (2021). Early Holocene cold snaps and their expression in the moraine record of the eastern European Alps. *Climate of the Past*, *17*(6), 2451–2479. https://doi.org/10.5194/cp-17-2451-2021

Chmeleff, J., von Blanckenburg, F., Kossert, K., & Jakob, D. (2010). Determination of the ^{10}Be half-life by multicollector ICP-MS and liquid scintillation counting. *Nuclear Instruments and Methods in Physics Research Section B: Beam Interactions with Materials and Atoms*, *268*(2), 192–199. https://doi.org/10.1016/j.nimb.2009.09.012

Conway, H., & Rasmussen, L. A. (2000). Summer temperature profiles within supraglacial debris on Khumbu Glacier, Nepal. *Debris-Covered Glaciers IAHS Publ. No. 264*, 89–97.

Finkel, R. C., Owen, L. A., Barnard, P. L., & Caffee, M. W. (2003). Beryllium-10 dating of Mount Everest moraines indicates a strong monsoon influence and glacial synchroneity throughout the Himalaya. *Geology*, *31*(6), 561–564. https://doi.org/10.1130/0091-7613(2003)031%3C0561:BDOMEM%3E2.0.CO;2

Gades, A., Conway, H., Nereson, N., Naito, N., & Kadota, T. (2000). Radio echo-sounding through supraglacial debris on Lirung and Khumbu Glaciers, Nepal Himalaya. In *Debris-Covered Glaciers: Proceedings of a workshop held at Seattle, Washington, USA* (No. 264, pp. 13–22). IAHS.

Godard, V., Bourles, D. L., Spinabella, F., Burbank, D. W., Bookhagen, B., Fisher, G. B., et al. (2014). Dominance of tectonics over climate in Himalayan denudation. *Geology*, *42*(3), 243–246. https://doi.org/10.1130/G35342.1

Hambrey, M. J., Quincey, D. J., Glasser, N. F., Reynolds, J. M., Richardson, S. J., & Clemmens, S. (2008). Sedimentological, geomorphological and dynamic context of debris-mantled glaciers, Mount Everest (Sagarmatha) region, Nepal. *Quaternary Science Reviews*, *27*(25–26), 2361–2389. https://doi.org/10.1016/j.quascirev.2008.08.010

Heimsath, A. M., & McGlynn, R. (2008). Quantifying periglacial erosion in the Nepal high Himalaya. *Geomorphology*, *97*(1–2), 5–23. https://doi.org/10.1016/j.geomorph.2007.02.046

Herber, L. (1969). Separation of feldspar from quartz by flotation. *American Mineralogist*, *54*, 1212–1216.

Herreid, S., & Pellicciotti, F. (2020). The state of rock debris covering Earth's glaciers. *Nature Geoscience*, *13*(9), 621–627. https://doi.org/10.1038/s41561-020-0615-0

Heyman, J., Applegate, P. J., Blomdin, R., Gribenski, N., Harbor, J. M., & Stroeven, A. P. (2016). Boulder height – Exposure age relationships from a global glacial ^{10}Be compilation. *Quaternary Geochronology*, *34*, 1–11. https://doi.org/10.1016/j.quageo.2016.03.002

Hugonnet, R., McNabb, R., Berthier, E., Menounos, B., Nuth, C., Girod, L., et al. (2021). Accelerated global glacier mass loss in the early twenty-first century. *Nature*, *592*(7856), 726–731. https://doi.org/10.1038/s41586-021-03436-z

Irvine-Fynn, T. D. L., Porter, P. R., Rowan, A. V., Quincey, D. J., Gibson, M. J., Bridge, J. W., et al. (2017). Supraglacial ponds regulate runoff from Himalayan debris-covered glaciers: Supraglacial ponds regulate runoff. *Geophysical Research Letters*, *44*, 11894–11904. https://doi.org/10.1002/2017GL075398

Kapannusch, R., Scherler, D., King, G., & Wittmann, H. (2020). Glacial influence on late Pleistocene ^{10}Be-derived paleo-erosion rates in the north-western Himalaya, India. *Earth and Planetary Science Letters*, *547*, 116441. https://doi.org/10.1016/j.epsl.2020.116441

King, O., Bhattacharya, A., Ghuffar, S., Tait, A., Guilford, S., Elmore, A. C., & Bolch, T. (2020). Six decades of glacier mass changes around Mt. Everest are revealed by historical and contemporary images. *One Earth*, *3*(5), 608–620. https://doi.org/10.1016/j.oneear.2020.10.019

Kirkbride, M. P. (2000). Ice-marginal geomorphology and Holocene expansion of debris-covered Tasman Glacier. *New Zealand, IAHSAISH P*, *264*, 211–217.

Kirkbride, M. P., & Winkler, S. (2012). Correlation of late Quaternary moraines: Impact of climate variability, glacier response, and chronological resolution. *Quaternary Science Reviews*, *46*, 1–29. https://doi.org/10.1016/j.quascirev.2012.04.002

Lifton, N., Sato, T., & Dunai, T. J. (2014). Scaling in situ cosmogenic nuclide production rates using analytical approximations to atmospheric cosmic-ray fluxes. *Earth and Planetary Science Letters*, *386*, 149–160. https://doi.org/10.1016/j.epsl.2013.10.052

Llliboutry, L. (1986). Discharge of debris by glaciar Hatunraju, Cordillera Blanca, Peru. *Journal of Glaciology*, *32*(110), 133. https://doi.org/10.1017/s002214300000695x

Maisch, M., Haeberli, W., Hoelzle, M., & Wenzel, J. (1999). Occurrence of rocky and sedimentary glacier beds in the Swiss Alps as estimated from glacier-inventory data. *Annals of Glaciology*, *28*, 231. https://doi.org/10.3189/172756499781821779

Mendelová, M., Hein, A. S., Rodés, Á., Smedley, R. K., & Xu, S. (2020). Glacier expansion in central Patagonia during the Antarctic Cold Reversal followed by retreat and stabilisation during the Younger Dryas. *Quaternary Science Reviews*, *227*, 106047. https://doi.org/10.1016/j.quascirev.2019.106047

Miles, K. E., Hubbard, B., Quincey, D. J., Miles, E. S., Sherpa, T. C., Rowan, A. V., & Doyle, S. H. (2018). Polythermal structure of a Himalayan debris-covered glacier revealed by borehole thermometry. *Scientific Reports*, *8*(1), 16825. https://doi.org/10.1038/s41598-018-34327-5

Murari, M. K., Owen, L. A., Dortch, J. M., Caffee, M. W., Dietsch, C., Fuchs, M., et al. (2014). Timing and climatic drivers for glaciation across monsoon-influenced regions of the Himalayan–Tibetan orogen. *Quaternary Science Reviews*, *88*, 159–182. https://doi.org/10.1016/j.quascirev.2014.01.013

Nicholson, L., & Benn, D. I. (2013). Properties of natural supraglacial debris in relation to modelling sub-debris ice ablation: Properties of supraglacial debris. *Earth Surface Processes and Landforms*, *38*(5), 490–501. https://doi.org/10.1002/esp.3299

Nicholson, L., Wirbel, A., Mayer, C., & Lambrecht, A. (2021). The challenge of non-stationary feedbacks in modeling the response of debris-covered glaciers to climate forcing. *Frontiers of Earth Science*, *9*, 662695. https://doi.org/10.3389/feart.2021.662695

Nishiizumi, K., Imamura, M., Caffee, M. W., Southon, J. R., Finkel, R. C., & McAninch, J. (2007). Absolute calibration of ^{10}Be AMS standards. *Nuclear Instruments and Methods in Physics Research Section B: Beam Interactions with Materials and Atoms*, *258*(2), 403–413. https://doi.org/10.1016/j.nimb.2007.01.297

Oerlemans, J. (1989). On the response of valley glaciers to climatic change. In J. Oerlemans (Ed.), *Glacier fluctuations and climatic change*, *Glaciology and Quaternary Geology* (pp. 353–371). Springer Netherlands. https://doi.org/10.1007/978-94-015-7823-3_23

Olen, S. M., Bookhagen, B., Hoffmann, B., Sachse, D., Adhikari, D. P., & Strecker, M. R. (2015). Understanding erosion rates in the Himalayan orogen: A case study from the Arun Valley. *Journal of Geophysical Research: Earth Surface*, *120*(10), 2080–2102. https://doi.org/10.1002/2014JF003410

Owen, L. A., & Dortch, J. M. (2014). Nature and timing of Quaternary glaciation in the Himalayan–Tibetan orogen. *Quaternary Science Reviews*, *88*, 14–54. https://doi.org/10.1016/j.quascirev.2013.11.016

Owen, L. A., Robinson, R., Benn, D. I., Finkel, R. C., Davis, N. K., Yi, C., et al. (2009). Quaternary glaciation of Mount Everest. *Quaternary Science Reviews*, *28*(15–16), 1412–1433. https://doi.org/10.1016/j.quascirev.2009.02.010

RGI Consortium. (2017). *Randolph glacier inventory – A dataset of global glacier outlines, version 6* (Indicate subset used). NSIDC: National Snow and Ice Data Center. https://doi.org/10.7265/4m1f-gd79

Richards, B. W. M. (2000). Luminescence dating of Quaternary sediments in the Himalaya and high Asia: A practical guide to its use and limitations for constraining the timing of glaciation. *Quaternary International*, *65*(66), 49–61. https://doi.org/10.1016/S1040-6182(99)00036-1

Richards, B. W. M., Benn, D. I., Owen, L. A., Rhodes, E. J., & Spencer, J. Q. (2000). Timing of late Quaternary glaciations south of Mount Everest in the Khumbu Himal, Nepal. *The Geological Society of America Bulletin*, *112*(10), 1621–1632. https://doi.org/10.1130/0016-7606(2000)112<1621:TOLQGS>2.0.CO;2

Rounce, D. R., King, O., McCarthy, M., Shean, D. E., & Salerno, F. (2018). Quantifying debris thickness of debris-covered glaciers in the Everest region of Nepal through inversion of a subdebris melt model. *Journal of Geophysical Research: Earth Surface*, *123*(5), 1094–1115. https://doi.org/10.1029/2017JF004395

Rowan, A. V. (2017). The 'Little Ice Age' in the Himalaya: A review of glacier advance driven by Northern Hemisphere temperature change. *The Holocene*, *27*(2), 292–308. https://doi.org/10.1177/0959683616658530

Rowan, A. V., Egholm, D. L., & Clark, C. D. (2022). Forward modelling of the completeness and preservation of palaeoclimate signals recorded by ice-marginal moraines. *Earth Surface Processes and Landforms*, *47*(9), 5371–2208. https://doi.org/10.1002/esp.5371

Rowan, A. V., Egholm, D. L., Quincey, D. J., & Glasser, N. F. (2015). Modelling the feedbacks between mass balance, ice flow and debris transport to predict the response to climate change of debris-covered glaciers in the Himalaya. *Earth and Planetary Science Letters*, *430*, 427–438. https://doi.org/10.1016/j.epsl.2015.09.004

Rowan, A. V., Egholm, D. L., Quincey, D. J., Hubbard, B., King, O., Miles, E. S., et al. (2021). The role of differential ablation and dynamic detachment in driving accelerating mass loss from a debris-covered Himalayan glacier. *Journal of Geophysical Research: Earth Surface*, *126*(9), e2020JF005761. https://doi.org/10.1029/2020JF005761

Saha, S., Owen, L. A., Orr, E. N., & Caffee, M. W. (2018). Timing and nature of Holocene glacier advances at the northwestern end of the Himalayan-Tibetan orogen. *Quaternary Science Reviews*, *187*, 177–202. https://doi.org/10.1016/j.quascirev.2018.03.009

Saha, S., Owen, L. A., Orr, E. N., & Caffee, M. W. (2019). High-frequency Holocene glacier fluctuations in the Himalayan-Tibetan orogen. *Quaternary Science Reviews*, *220*, 372–400. https://doi.org/10.1016/j.quascirev.2019.07.021

Saha, S., Sharma, M. C., Murari, M. K., Owen, L. A., & Caffee, M. W. (2016). Geomorphology, sedimentology and minimum exposure ages of streamlined subglacial landforms in the NW Himalaya, India. *Boreas*, *45*(2), 284–303. https://doi.org/10.1111/bor.12153

Scherler, D. (2014). Climatic limits to headwall retreat in the Khumbu Himalaya, eastern Nepal. *Geology*, *42*(11), 1019–1022. https://doi.org/10.1130/G35975.1

Scherler, D., Bookhagen, B., & Strecker, M. R. (2011). Hillslope-glacier coupling: The interplay of topography and glacial dynamics in High Asia. *Journal of Geophysical Research*, *116*(F2), F02019. https://doi.org/10.1029/2010JF001751

Scherler, D., & Egholm, D. L. (2020). Production and transport of supraglacial debris: Insights from cosmogenic ^{10}Be and numerical modeling, Chhota Shigri Glacier, Indian Himalaya. *Journal of Geophysical Research: Earth Surface*, *125*, e2020JF005586. https://doi.org/10.1029/2020JF005586

Searle, M. P., Simpson, R. L., Law, R. D., Parrish, R. R., & Waters, D. J. (2003). The structural geometry, metamorphic and magmatic evolution of the Everest massif, High Himalaya of Nepal–South Tibet. *Journal of Geological Society*, *160*(3), 345–366. https://doi.org/10.1144/0016-764902-126

Shean, D. (2017). *High Mountain Asia 8-meter DEM mosaics derived from optical imagery, version 1*. NASA National Snow and Ice Data Center Distributed Active Archive Center. https://doi.org/10.5067/KXOVQ9L172S2

Smith, M. J., & Clark, C. D. (2005). Methods for the visualization of digital elevation models for landform mapping. *Earth Surface Processes and Landforms*, *30*(7), 885–900. https://doi.org/10.1002/esp.1210

Solomina, O. N., Bradley, R. S., Hodgson, D. A., Ivy-Ochs, S., Jomelli, V., Mackintosh, A. N., et al. (2015). Holocene glacier fluctuations. *Quaternary Science Reviews*, *111*, 9–34. https://doi.org/10.1016/j.quascirev.2014.11.018

Solomina, O. N., Bradley, R. S., Jomelli, V., Geirsdottir, A., Kaufman, D. S., Koch, J., et al. (2016). Glacier fluctuations during the past 2000 years. *Quaternary Science Reviews*, *149*, 61–90. https://doi.org/10.1016/j.quascirev.2016.04.008

Xu, S., Dougans, A. B., Freeman, S. P. H. T., Schnabel, C., & Wilcken, K. M. (2010). Improved ^{10}Be and ^{26}Al-AMS with a 5 MV spectrometer. *Nuclear Instruments and Methods in Physics Research Section B: Beam Interactions with Materials and Atoms*, *268*(7–8), 736–738. https://doi.org/10.1016/j.nimb.2009.10.018

Zemp, M., Kääb, A., Hoelzle, M., & Haeberli, W. (2005). GIS-based modelling of glacial sediment balance. *Zeitschrift für Geomorphologie*, *138*, 113–129. https://doi.org/10.5167/UZH-40580